Mixed-lubrication analysis of misaligned journal bearing considering turbulence and cavitation

Xintao Song ; Wei Wu ; Shihua Yuan

Check for updates

CrossMark

View Online   Export Citation

Articles You May Be Interested In

Experimental investigation of single cylinder DI diesel engine by diesel–JFO and its blends

AIP Conference Proceedings (December 2020)

Investigation of two-phase change flow in mechanical seal with complex solid surfaces

AIP Advances (June 2019)

The Olsson sum rule and the rho Regge pole

AIP Conference Proceedings (February 2007)
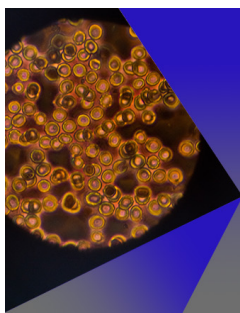
Mixed-lubrication analysis of misaligned journal bearing considering turbulence and cavitation

View Online   Export Citation   CrossMark

Xintao Song, 🄳 Wei Wu,a) 🄳 and Shihua Yuan

AFFILIATIONS

School of Mechanical Engineering, Beijing Institute of Technology, Beijing 100081, China

a)Author to whom correspondence should be addressed: wuweijing@bit.edu.cn

ABSTRACT

By integrating the average flow equation and Ng–Pan turbulence model using the boundary condition of mass conserving [Jakobsson-Floberg-Olsson (JFO)], a mixed lubrication model for misaligned bearing was established considering the effects of turbulence and cavitation. The numerical solution was obtained using a finite difference scheme. The results indicate that the frictional force and moment calculated using the JFO boundary condition are greater than those calculated using the Reynolds boundary condition under the constant external load. In high speed conditions, the turbulence begins to play a role, which makes the maximum oil film pressure and moment decrease and the minimum oil film thickness, cavitation zone, and friction coefficient increase. The boundary condition and turbulence have important effects on the equilibrium position of the axis. The misalignment leads to an obvious increase in the friction of the mixed lubrication area and a slight decrease in that of the hydrodynamic lubrication area.

I. INTRODUCTION

Journal bearings are widely used in a variety of rotating machineries, such as wind power, turbine, and ship stern shaft, and their tribological properties directly affect the safety and reliability of the rotor system. Due to manufacturing errors, installation errors, and uneven load, journal misalignment is inevitable. Scholars have done a lot of work on the misalignment. Sun and Gui[1] studied the influence of shaft deformation on the full film lubrication performance of bearing and found that journal misalignment has important effects on the oil film pressure distribution, oil film thickness distribution, and moment. In the case of the large eccentricity ratio and misalignment angle, the moment to maintain the stable operation of bearing increases significantly. Manser et al.[2] comprehensively discussed the influence of misalignment on the tribological performance of surface textured bearing. The results show that as the misalignment degree (D_m) increases, the maximum hydrodynamic pressure, friction force, and moment all increase. Guo et al.[3] established a transient lubrication model to study the influences of misalignment and axial movement on the performance of groove shaped textured bearing. Ma et al.[4] discussed the influences of surface roughness and misalignment on the performance

of hydrodynamic lubricated bearing. Jang and Khonsari[5] reviewed the variation of bearing performance caused by misalignment and emphasized that misalignment is detrimental to bearing performance. However, the above research did not consider the influence of misalignment on the lubrication performance of the bearing in the mixed lubrication (ML) state. de Kraker et al.[6] established the mixed lubrication model of water-lubricated bearing through the average Reynolds equation[7] and calculated the Stribeck curve of the bearing. Lv et al.[8,9] studied the effect of misalignment on the mixed lubrication performance of bearing and found that the misalignment leads to the rise in the friction coefficient, which requires a higher speed to enter hydrodynamic lubrication (HL) from mixed lubrication (ML).

High velocity, large clearance, and low viscosity lubricants may cause turbulence. Turbulence models commonly used in lubrication analysis include Constantinescu,[10] Ng–Pan,[11] Elrod–Ng,[12] and Hirs.[13] Dousti et al.[14] used the Constantinescu model to analyze the influences of turbulence and inertia force on bearing performance. The research showed that turbulence increases the bearing capacity and attitude angle and decreases the eccentricity. Feng et al.[15] investigated the influence of turbulence on the misaligned bearing performance through the Ng–Pan model and found that turbulence improves the bearing capacity. Lv et al.[9] discussed the influence

of turbulence on the lubrication performance of misaligned bearing under the condition of constant load and found that turbulence reduces the maximum hydrodynamic pressure and increases the friction coefficient. Awasthi and Maan[16] discussed the effect of turbulence on the performance of textured hydrodynamic lubricated bearing. At the same time, the boundary conditions have an important influence on the simulation results. The commonly used boundary conditions for lubrication analysis are the Reynolds boundary condition[17] and [Jakobsson-Floberg-Olsson (JFO)] boundary condition,[18,19] and the latter is more accurate. Later, Elrod[20] and Payvar and Salant[21] improved the cavitation algorithm. Jang and Khonsari[22] used the Elrod algorithm to study the tribological performance of misaligned bearing. He *et al.*[23] compared the friction coefficients under the two boundary conditions and found that the friction coefficient calculated using the JFO condition is greater than the result of the Reynolds condition. Lin *et al.*[24] studied the effects of cavitation and turbulence on the thrust water-lubricated bearing performance and found that cavitation reduces the bearing capacity, and turbulence increases the bearing capacity. However, the research on the effects of turbulence and cavitation on the mixed lubrication performance of misaligned journal bearing is still lacking.

Based on the average flow equation and turbulence model, a mixed lubrication model for misalignment bearing is established considering turbulence and cavitation. The finite difference scheme is used to solve the model. The effects of turbulence, cavitation, and misalignment on the mixed lubrication performance of bearing are studied. The research results can provide reference for journal bearing design.

II. GOVERNING EQUATION

A. Film thickness equation

Figure 1 displays the schematic diagram and coordinate system of a misaligned bearing. The film thickness equation is

$$h = c + e_0 \cos(\theta - \varphi_0) + e'\left(\frac{y}{L} - \frac{1}{2}\right)\cos(\theta - \alpha - \varphi_0), \quad (1)$$

where c is the radial clearance, e_0 is the eccentricity at the bearing middle plane, φ_0 is the attitude angle, e' is the projection of the axis, α is the misalignment angle, and L is the bearing length.
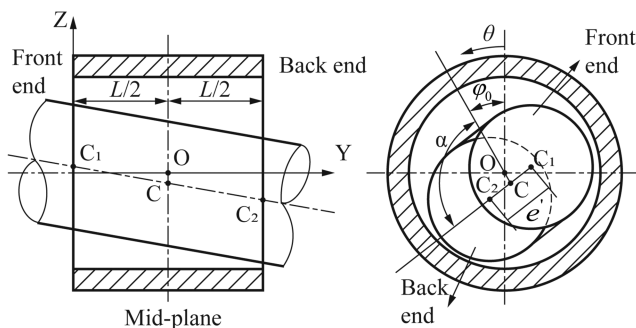

FIG. 1. Schematic diagram of a misaligned journal bearing.

The dimensionless equation (1) can be obtained as the following expression:

$$\bar{h} = 1 + \varepsilon_0 \cos(\theta - \varphi_0) + \varepsilon'\left(\frac{y}{L} - \frac{1}{2}\right)\cos(\theta - \alpha - \varphi_0), \quad (2)$$

where ε_0 is the eccentricity ratio and ε' is the misalignment eccentricity ratio, which can be computed from Ref. 25 as follows:

$$\varepsilon' = \frac{e'}{c} = D_m \varepsilon'_{max}, \quad (3)$$

where ε'_{max} is the maximum possible value of ε', which can be written as

$$\varepsilon'_{max} = 2\left(\sqrt{1 - \varepsilon_0^2 \sin^2(\alpha)} - \varepsilon_0|\cos(\alpha)|\right). \quad (4)$$

B. Generalized lubrication equation

The average Reynolds equation was proposed by Patir and Cheng.[7] Using the cavitation algorithm proposed by Payvar and Salant,[21] the laminar lubrication equation considering the JFO cavitation effect is obtained as follows:

$$\frac{\partial}{\partial x}\left(\phi_x \frac{h^3}{12\eta}\frac{\partial(F\phi)}{\partial x}\right) + \frac{\partial}{\partial y}\left(\phi_y \frac{h^3}{12\eta}\frac{\partial(F\phi)}{\partial y}\right)$$
$$= \frac{U\phi_c}{2(p_{ref} - p_c)}\frac{\partial\{[1 + (1 - F)\phi]h\}}{\partial x} + \frac{UF\sigma}{2(p_{ref} - p_c)}\frac{\partial\phi_s}{\partial x}, \quad (5)$$

where ϕ_x and ϕ_y are the pressure flow factors, ϕ_s is the shear flow factor,[7] ϕ_c is the contact factor,[26] η is the viscosity of lubricating oil, σ is the effective roughness, h is the nominal film thickness, p_c is the cavitation pressure, p_{ref} is the reference pressure, F is the cavitation index, ϕ is the dimensionless pressure in the full film zone, $(1 + \phi)$ is the partial film content in the cavitation zone, and U is the journal speed.

According to the turbulence model proposed by Ng and Pan,[11] the turbulent lubrication equation considering the JFO cavitation effect can be derived, as shown in the Appendix, and its expression is

$$\frac{\partial}{\partial x}\left(\phi_x \frac{h^3}{k_x}\frac{\partial(F\phi)}{\partial x}\right) + \frac{\partial}{\partial y}\left(\phi_y \frac{h^3}{k_y}\frac{\partial(F\phi)}{\partial y}\right)$$
$$= \frac{\eta U\phi_c}{2(p_{ref} - p_c)}\frac{\partial\{[1 + (1 - F)\phi]h\}}{\partial x} + \frac{\eta UF\sigma}{2(p_{ref} - p_c)}\frac{\partial\phi_s}{\partial x}, \quad (6)$$

where k_x and k_y are the turbulent factors,

$$\begin{cases} k_x = 12(1 + 0.0013R_L^{0.9}), & R_L > R_c, \\ k_y = 12(1 + 0.000\,358R_L^{0.96}), & R_L > R_c, \\ k_x = k_y = 12, & R_L \leq R_c, \end{cases} \quad (7)$$

where R_L and R_c are the local Reynolds number and critical Reynolds number, respectively. The expression of R_c is $R_c = 41.1\sqrt{R/c}$, where R is the radius of the shaft.

The mean hydrodynamic pressure is

$$p = p_c + F\phi(p_{ref} - p_c). \quad (8)$$

The fluid bearing capacity can be obtained using the integral equation (8), and the capacity components in x and z coordinates are

$$\begin{cases} F_{\text{oil}x} = -\iint\limits_{A} p \, \sin \theta dA, \\ F_{\text{oil}z} = -\iint\limits_{A} p \, \cos \theta dA, \end{cases} \tag{9}$$

where A is the unfolded area of the bearing.

C. Asperity contact force

In some working conditions, the minimum film thickness is less than the rough peak height. Therefore, the bearing surface and journal surface inevitably come into contact. The contact force and oil film force share the external load. Using the asperity contact model put forward by Greenwood and Trip,[27] the contact pressure is

$$p_{\text{asp}} = \frac{16\sqrt{2}}{15} \pi (\eta_s \beta \sigma)^2 E' \sqrt{\frac{\sigma}{\beta}} \cdot F_{5/2}(\lambda), \tag{10}$$

where η_s is the density of asperity, β is the effective asperity radius, E' is the equivalent elastic modulus, λ is the film thickness ratio ($\lambda = h/\sigma$), and $F_{2.5}(\lambda)$ is the statistical function that the height of the asperity obeys the Gaussian distribution, and its expression is[28]

$$F_{5/2}(\lambda) = \begin{cases} 4.4086 \cdot 10^{-5}(4-\lambda)^{6.804} & (\lambda \le 4), \\ 0 & (\lambda > 4). \end{cases} \tag{11}$$

The asperity contact force in the x-axis and z-axis is

$$\begin{cases} F_{\text{asp}x} = -\iint\limits_{A} p_{\text{asp}} \, \sin \theta dA, \\ F_{\text{asp}z} = -\iint\limits_{A} p_{\text{asp}} \, \cos \theta dA. \end{cases} \tag{12}$$

D. Friction coefficient

Considering the influence of turbulence, the shear stress of lubricating oil is

$$\tau = -\frac{k_\tau \eta U}{h}(\phi_f - \phi_{fs}) - \phi_{fp} \frac{h}{2} \frac{\partial p}{\partial x}, \tag{13}$$

where ϕ_f, ϕ_{fs}, and ϕ_{fp} are the shear stress factors[29] and k_τ is the turbulent factor,

$$\begin{cases} k_\tau = 1 + 0.0012 R_L^{0.94}, & R_L > R_c, \\ k_\tau = 1, & R_L \le R_c. \end{cases} \tag{14}$$

The friction force of fluid shear is

$$F_{\text{foil}} = \iint\limits_{A} \tau dA. \tag{15}$$

The expression of contact friction force is

$$F_{\text{fasp}} = \iint\limits_{A} f_{\text{asp}} p_{\text{asp}} dA, \tag{16}$$

where f_{asp} is the boundary friction coefficient of the two surfaces.

The total bearing friction can be obtained by summing Eqs. (15) and (16), and the expression is

$$F_f = F_{\text{foil}} + F_{\text{fasp}}. \tag{17}$$

The total friction coefficient is

$$f = F_f/W. \tag{18}$$

E. Misalignment moment

The moments in the two coordinate axis directions are

$$\begin{cases} M_x = \int_0^L \int_0^{2\pi} (p + p_{\text{asp}})\left(y - \frac{L}{2}\right) R \, \cos \theta d\theta dy, \\ M_z = \int_0^L \int_0^{2\pi} (p + p_{\text{asp}})\left(y - \frac{L}{2}\right) R \, \sin \theta d\theta dy. \end{cases} \tag{19}$$

The total moment is

$$M = \sqrt{M_x^2 + M_z^2}. \tag{20}$$

III. NUMERICAL SOLUTION AND MODEL VALIDATION

A. Numerical solution

In order to solve the above equations, a specific numerical solution flow as shown in Fig. 2 is established. The detailed solution steps are as follows:

(1) Assume the initial position of the axis, i.e., initial eccentricity ratio ε_0 and attitude angle φ_0.
(2) Calculate the dimensionless oil film thickness according to Eq. (2).
(3) Calculate the Reynolds number and turbulence coefficient according to the obtained parameters.
(4) Solve the Reynolds equation (6) to obtain the independent variable ϕ; if it converges, it goes to next, else, it returns step (3).
(5) Calculate oil film force and asperity contact force using Eqs. (9) and (12), respectively.
(6) The equilibrium position of the axis is obtained using the balance of oil film force, asperity contact force, and external force.
(7) Output bearing performance.

B. Validation

The program verification includes three parts, namely, cavitation model verification, journal misalignment verification, and mixed lubrication model verification. The results correspond to Figs. 3–5, respectively. Figure 3 shows the comparison between the calculated hydrodynamic pressure at 1/5 and 3/5 from the bearing center and experimental results in Ref. 18. The theoretical calculation results are consistent with those obtained by experiments, indicating that the model is correct. Figure 4 presents the comparison between the calculated moment in this paper and that in Ref. 1. The two calculation results are in good agreement. Figure 5 displays the comparative study between the friction coefficients
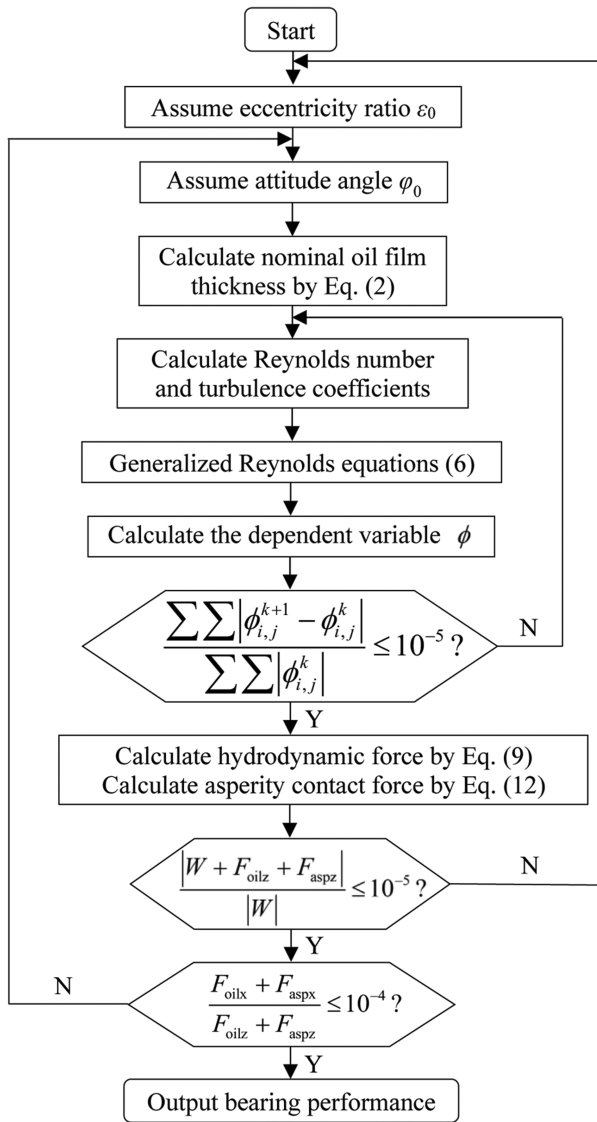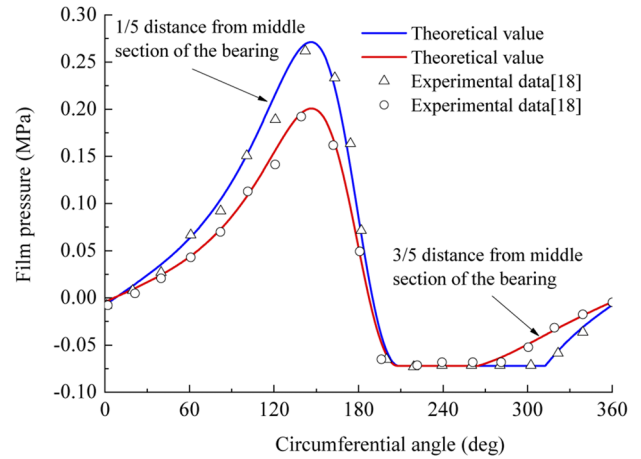
FIG. 2. Numerical calculation flowchart.

FIG. 3. Comparison between calculated oil film pressure and experimental results.

different boundary conditions when n = 200 rpm. Compared with the Reynolds boundary condition, the maximum hydrodynamic pressure and minimum oil film thickness calculated using the JFO boundary condition move downstream, namely, the attitude angle calculated using the JFO boundary condition is larger than that calculated using the Reynolds boundary condition. In the divergent region of oil wedge, the oil film breaks and cavitation occurs inevitably. Cavitation will produce a negative pressure zone below atmospheric pressure, as shown in Fig. 6(a), which cannot provide bearing capacity. The Reynolds boundary condition takes atmospheric pressure as cavitation pressure, and the pressure gradient is set to zero in the oil film break region. Therefore, the Reynolds boundary condition will generate greater errors in comparison with the results calculated using the JFO boundary condition.

Figure 7 displays the variation in film pressure and thickness distributions in the middle section with speed. As the rotation speed
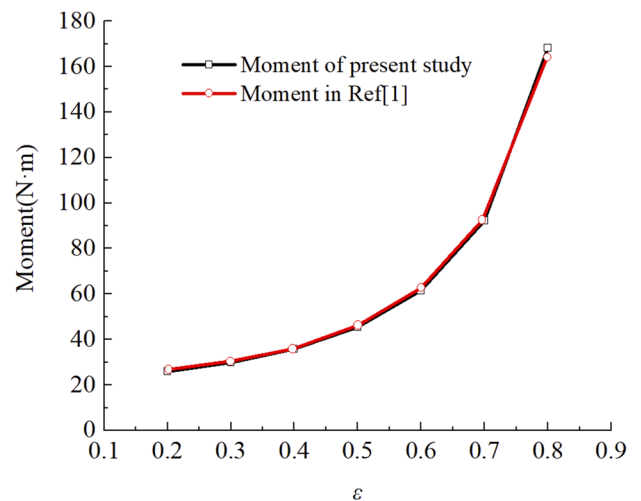
using the present model and that from Ref. 8. The two are very close, and the slight difference may be related to the number of meshes and the selection of convergence accuracy.

IV. RESULTS AND DISCUSSION

The parameters used in this paper are shown in Table I, which are mainly derived from Ref. 9. The external load is taken as a constant value.

A. Effect of boundary conditions

Figure 6 shows the comparison of oil film pressure and thickness distributions in the mid-plane of bearing under

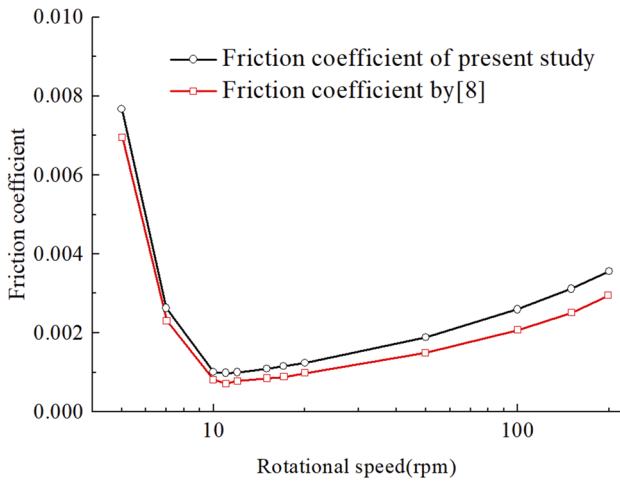FIG. 4. Comparison of moment calculation results.

FIG. 5. Friction coefficient for different models.

increases, the maximum film pressure decreases, while the fluid bearing area, cavitation area, and minimum film thickness increase. The maximum oil film pressure and the minimum oil film thickness move downstream. That is to say, the attitude angle increases, while

the eccentricity ratio decreases when the speed increases. The main reason is that the hydrodynamic effect is enhanced at high speed, which causes the bearing capacity to improve, so it can be balanced with the external load under small eccentricity.

Figure 8 presents the variation in the axial position of aligned bearing with speed under two boundary conditions. In the case of misalignment, the change in the axial position obtained from the two boundary conditions with speed is similar to that of alignment, so it is no longer shown in Fig. 8. When the rotation speed is 10 rpm, the eccentricity ratio and attitude angle corresponding to Reynolds and JFO conditions are 0.9951 and 5.41°, and 0.9952 and 7.59°, respectively, and when the rotation speed is 200 rpm, the corresponding eccentricity ratio and attitude angle are 0.9297 and 25.93°, and 0.931 and 36.69°, respectively. It can be clearly found that at the same speed, the eccentricity ratio and attitude angle calculated using the JFO boundary condition are larger than those calculated using the Reynolds boundary condition. In addition, with the increase in speed, the difference of the axial position calculated using the two boundary conditions is greater. The reason for this is that when the speed increases, the cavitation area increases [see Fig. 7(a)], and the influence of cavitation on the bearing capacity increases. It is worth noting that, under the JFO boundary condition, a greater eccentricity ratio is needed to guarantee balance with a constant external load, which increases the

TABLE I. Parameters for the calculated bearing.

| Parameters	Values	Parameters	Values
Radius (mm)	400	Bearing length/diameter ratio	2
Radial clearance (mm)	1.52	Speed (rpm)	0–200
Roughness of two surfaces (μm)	4.3	Poisson ratio of the shaft and bush	0.3/0.34
Elastic modulus of bush (Pa)	1.0×10^{11}	Elastic modulus of the shaft (Pa)	2.1×10^{11}
External applied load (kN)	320	Viscosity (Pa s)	0.011
Boundary friction coefficient	0.1	Cavitation pressure (Pa)	−72 139.79
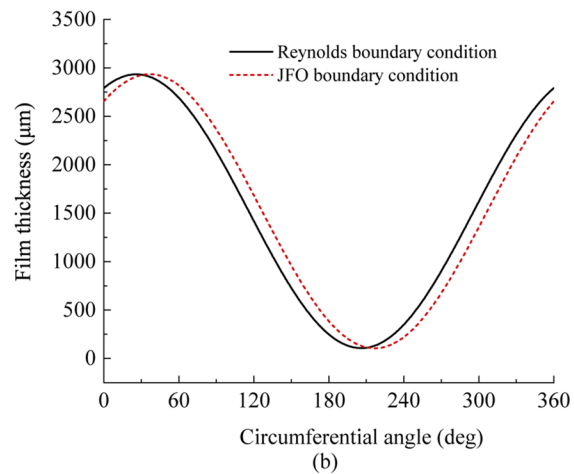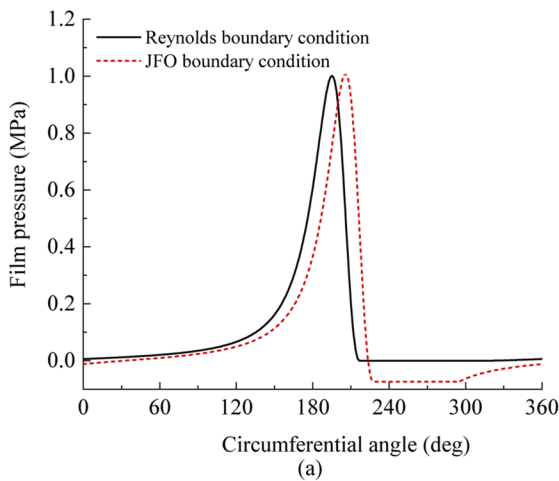
FIG. 6. Comparison of film pressure and thickness distributions in the middle section of the bearing under different boundary conditions (*n* = 200 rpm): (a) film pressure and (b) film thickness.
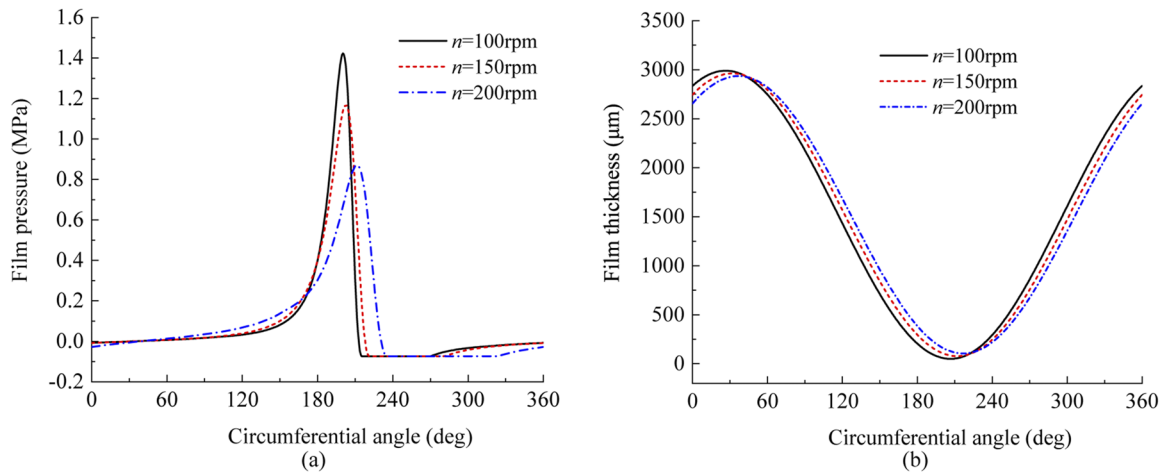
FIG. 7. Film pressure and thickness in the mid-plane of the bearing vs speed: (a) film pressure and (b) film thickness.

possibility of contact between the two surfaces and causes bearing wear failure.

Figure 9 shows the Stribeck curves under different boundary conditions for both aligned and misaligned bearing. No matter whether the journal is misaligned or not, the friction coefficient calculated using the JFO boundary condition is greater than that calculated using the Reynolds boundary condition. In the case of alignment, the speeds corresponding to the minimum friction coefficient under JFO boundary and Reynolds boundary conditions are 28 and 25 rpm, respectively. In the case of misalignment, the critical speeds are 68 and 65 rpm, respectively. Compared with the curve calculated using the Reynolds boundary condition, the curve calculated using the JFO boundary condition requires a higher speed to transform from the ML to HL state for both aligned and misaligned bearing. This is because in the oil film rupture area, the hydrodynamic pressure obtained using the JFO boundary condition has a negative pressure zone, as shown in Fig. 6(a), which causes the bearing capacity to decrease. At the same speed, the JFO boundary condition requires a higher eccentricity to balance the external load compared with the Reynolds boundary condition (see Fig. 8), leading to the increase in the friction coefficient. Compared with the alignment case, the misalignment causes the friction coefficient to increase evidently in the ML stage and decrease slightly in the HL stage in both boundary conditions. The critical speed of misalignment is much greater than that of alignment. This is because the
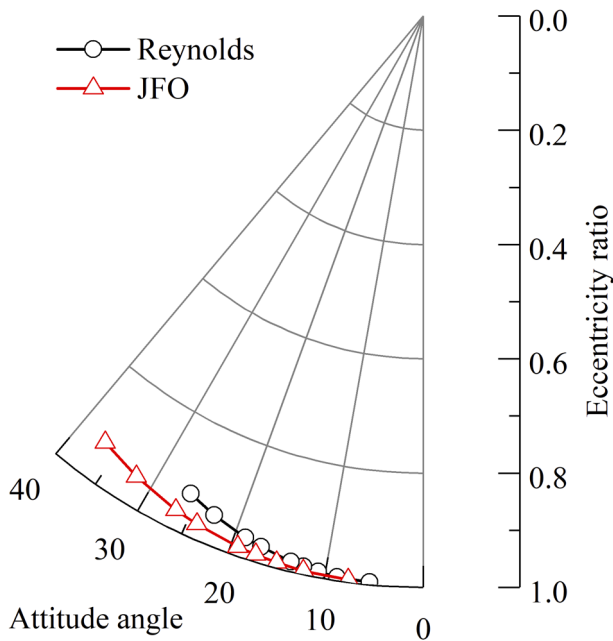

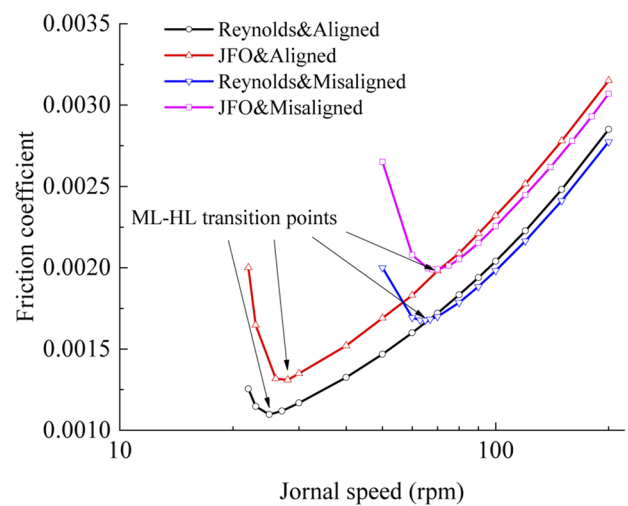**FIG. 8.** Variation in the axial position under different boundary conditions.

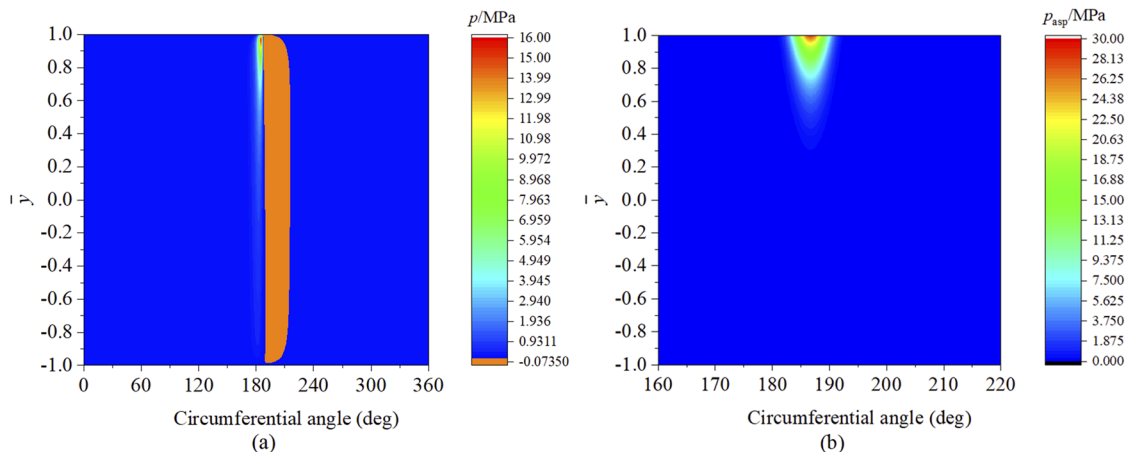**FIG. 9.** Effect of the boundary condition on the Stribeck curve.

FIG. 10. Oil film pressure and asperity contact pressure distributions along circumferential and axial directions (n = 10 rpm): (a) film pressure and (b) contact pressure.

misalignment leads to a sharp increase in the asperity contact pressure and hydrodynamic pressure at one end of the bearing in the ML state, as shown in Fig. 10, which eventually causes the friction force to increase.

Figure 11 shows the variation in the moment with speed under different boundary conditions. In the two cases of misalignment, the moment calculated using the JFO boundary condition is greater than that calculated using the Reynolds boundary condition. The moment corresponding to D_m equal to 0.8 is greater than that when D_m is 0.6. In the case of a large degree of misalignment, the overturning moment becomes larger. As the speed increases, the moment obtained using the two boundary conditions decreases, and the
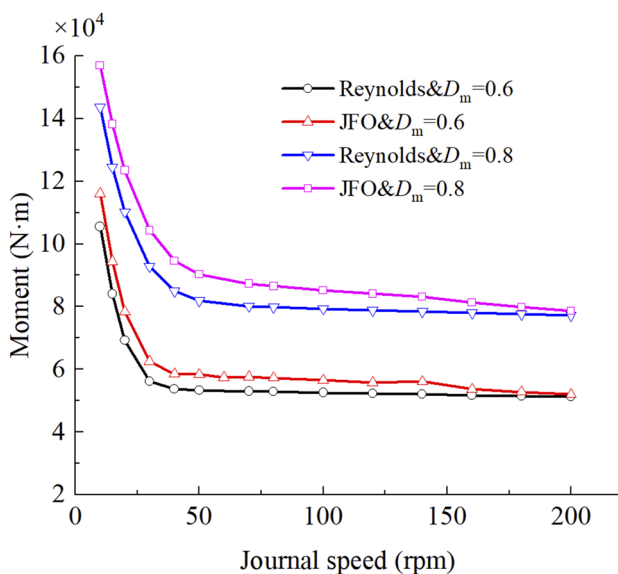
moment difference between the two boundary conditions decreases gradually. When the rotation speed is 10 and 200 rpm, the moment difference percentage between the two boundary conditions is 8.51% and 1.86%, respectively. It can be interpreted that when the journal speed is low, the film thickness is small to ensure that it can be balanced with the external load, resulting in a sharp increase in the hydrodynamic pressure and contact pressure at one end of bearing, so the moment is larger. See Fig. 10; the maximum hydrodynamic pressure and contact pressure are close to 16 and 30 MPa, respectively, and they are concentrated at one end of bearing, which inevitably leads to a large moment. Under high-speed operating conditions, the bearing capacity is enhanced and the film thickness is increased, resulting in a more uniform distribution of film pressure along the bearing width, so the moment decreases. In general, boundary conditions have important effects on pressure distribution, film thickness distribution, axial position, friction coefficient, and moment. Therefore, it is very important to deal with the cavitation boundary, which will have a major impact influence on the bearing performance.

B. Effect of turbulence

Figure 12 presents the film pressure distributions under four different conditions when n = 200 rpm and D_m = 0.8. The maximum film pressures correspond to Figs. 12(a)–12(d) are 1.01, 0.87, 3.33, and 2.69 MPa, respectively. It can be found that regardless of whether misalignment is considered, turbulence makes the maximum film pressure drop and the cavitation zone increase. No matter whether turbulence is considered or not, the misalignment makes the oil film pressure unevenly distributed along the axis; moreover, the maximum film pressure is far away from the middle section and moves to one end of the bearing. Meanwhile, the misalignment also makes the maximum film pressure increase sharply.

Figures 13 and 14 illustrate the hydrodynamic pressure and film thickness distributions in the middle section of the bearing when
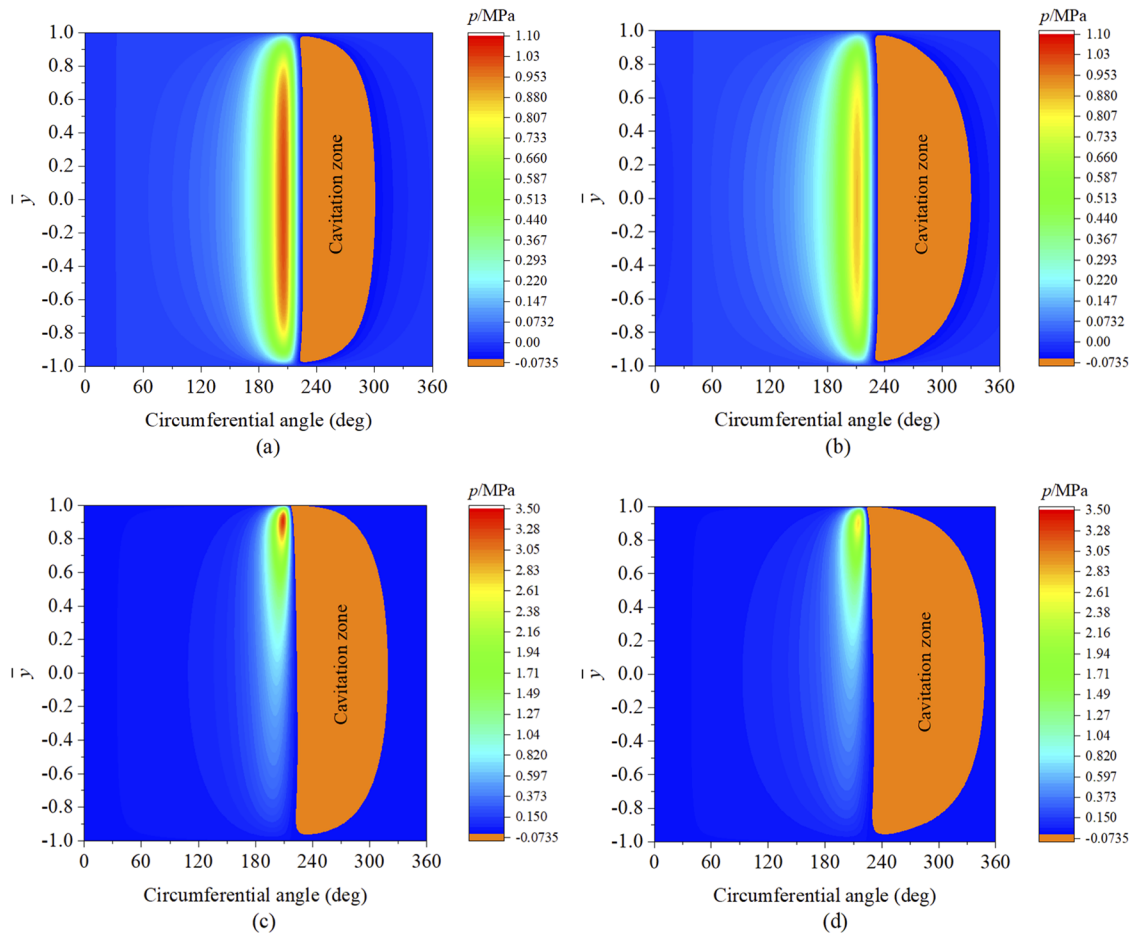

FIG. 11. Effect of the boundary condition on moment.

FIG. 12. Effects of turbulence and misalignment on film pressure along circumferential and axial directions: (a) laminar and aligned, (b) turbulent and aligned, (c) laminar and misaligned, and (d) turbulent and misaligned.

n = 200 rpm and D_m = 0.8, respectively. From Fig. 13, it is noted that no matter whether the misalignment is considered or not, turbulence reduces the maximum hydrodynamic pressure and widens the hydrodynamic region compared with laminar flow. The reason is that turbulence increases the minimum film thickness; see the partial enlarged view of Fig. 14, whether the effect of misalignment is considered or not. The minimum film thicknesses corresponding to the four cases of A, B, C, and D are 105.2, 120.2, 136.2, and 154.7 μm, respectively. Meanwhile, turbulence makes the maximum hydrodynamic pressure and the minimum film thickness move downstream (see Figs. 13 and 14). Compared with laminar flow, turbulent flow makes the bearing balance with external load at a smaller eccentricity ratio. In other words, turbulence enhances the load capacity of the bearing.

Figure 15 displays the effect of turbulence on the axial position in the case of journal alignment. When the speed is less than 80 rpm, the axial positions obtained by the laminar flow model and turbulence model coincide, that is, no turbulence occurs. However, when the speed is above 80 rpm, turbulence significantly changes the

position of the shaft center. It should be noticed that the higher the rotation speed is, the larger the influence of turbulence on the axial position is; especially, n is equal to 200 rpm. When the rotation speed is equal to 200 rpm, the eccentricity ratio and attitude angle corresponding to the laminar and turbulent models are 0.931 and 36.69°, and 0.921 and 43.38°, respectively. Turbulence causes the attitude angle of bearing to increase obviously and the eccentricity ratio to decrease slightly.

Figure 16 shows the effects of turbulence and misalignment on the Stribeck curve of the bearing. No matter whether the journal is misaligned or not, when the speed is less than 70 rpm, no turbulence occurs, and the friction coefficients calculated by the laminar and turbulent models are equal. The critical speeds of the transition from ML to HL in the case of alignment and misalignment are 28 and 68 rpm, respectively, for both flow regimes. However, with the increasing journal speed, especially when it exceeds 80 rpm, the influence of turbulence on friction becomes significant. Compared with laminar flow, turbulent flow increases the friction coefficient of the bearing. This is because turbulent flow causes the fluid shear stress to increase
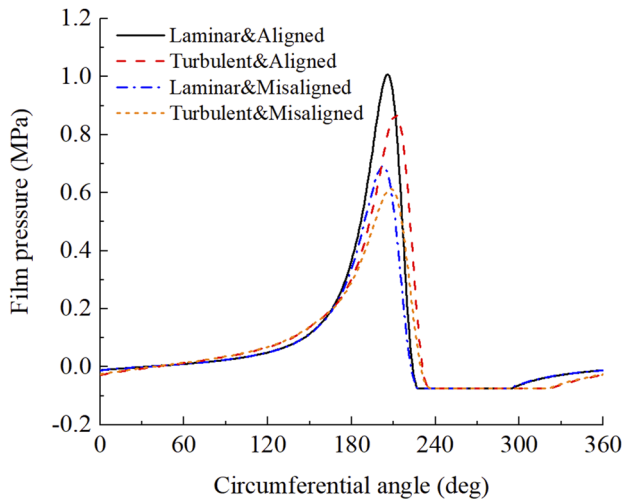
18 September 2023 09:20:15

FIG. 13. Effect of turbulence on hydrodynamic pressure distributions in the mid-plane of bearing.
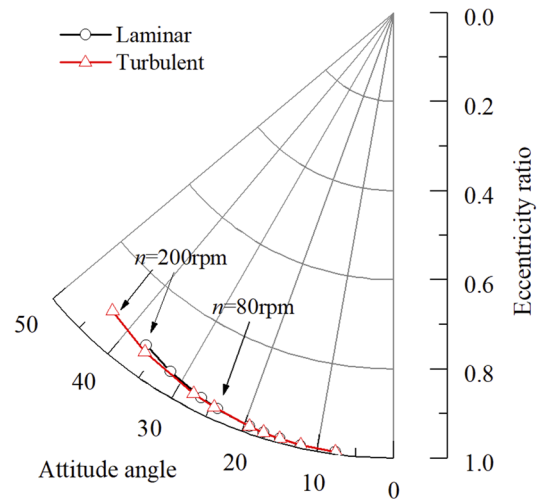

FIG. 15. Effect of turbulence on the axial position.

[see Eq. (13)], and the turbulence only occurs in the HL area. When the speed increases, the Reynolds number R_L and turbulence factor k_τ increase, causing the friction force to increase. The critical speed from laminar to turbulent flow is 70 rpm. The journal misalignment results in the increase in the friction coefficient in the ML stage and the decrease in the friction coefficient in the HL stage in both laminar flow and turbulent flow regimes in comparison to the alignment case. The reasons have been explained in Sec. IV A and will not be repeated here.

Figure 17 shows the effect of turbulence on moment when the misalignment degree D_m is 0.6 and 0.8. It can be found that when the speed is less than 70 rpm, the moment calculated by the turbulent flow model and the laminar flow model is equal, that is, no turbulence occurs. When the speed is greater than 70 rpm, turbulence occurs, causing the moment to decrease slightly. As the speed

increases, the rate of moment drop significantly increases. This is because turbulent flow makes the maximum film pressure decrease and the pressure distribution more uniform, as shown in Figs. 12(c) and 12(d). At high speed, the effect of turbulence on moment is more obvious. When the speed is equal to 100 rpm and D_m is 0.6 and 0.8, the corresponding moment drop percentages are 1.44% and 1.38%, respectively, and when the speed is equal to 200 rpm, the corresponding moment drop percentages are 12.95% and 12.68%, respectively.

From the analysis of Figs. 12–17, it can be seen that under high-speed working conditions, turbulence has a significant impact on the bearing lubrication characteristics. Therefore, under high-speed working conditions and large clearance, the design of the bearing must consider the influence of turbulence.
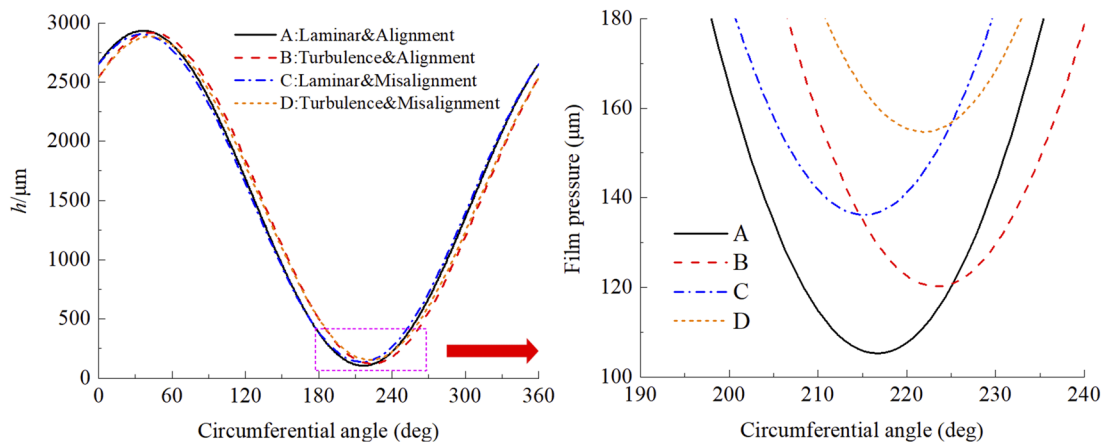

FIG. 14. Effect of turbulence on film thickness distribution in the mid-plane of bearing.
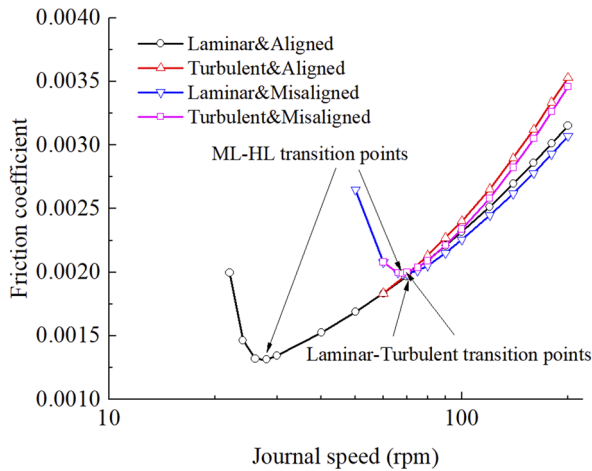
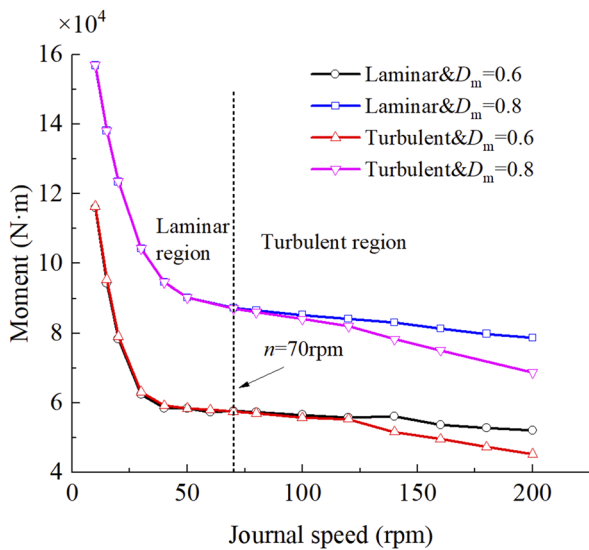**FIG. 16.** Effects of turbulence and misalignment on Stribeck curves.

FIG. 17. Effect of turbulence on moment.

V. CONCLUSIONS

In this paper, a mixed lubrication model of misalignment bearing considering cavitation and turbulence is established. The effects of cavitation, turbulence, and misalignment on the lubrication performance of bearing are analyzed, and the following conclusions are obtained:

(1) Under the condition of constant external load, boundary conditions have significant effects on the film pressure distribution, film thickness distribution, axial position, friction coefficient, and moment. Both the eccentricity ratio and attitude angle calculated using the Reynolds boundary condition are smaller than those obtained using the JFO boundary condition, and the friction coefficient and moment are underestimated under the Reynolds boundary condition. Under

the high-speed condition, the position difference between the two axes increases and the percentage of moment difference decreases.

(2) Turbulence occurs at high speed, which reduces the maximum film pressure and moment and increases the minimum film thickness, cavitation area, and friction coefficient. Turbulence causes the bearing attitude angle to increase obviously and the eccentricity ratio to decrease slightly. The higher the speed is, the greater the difference in the axial position and moment drop percentage are. Turbulence increases the load capacity of the bearing. Under the conditions of high speed and large clearance, the bearing design cannot ignore the turbulence factor.

(3) Compared with the case of alignment, the misalignment degree D_m reduces the minimum film thickness and increases the maximum hydrodynamic pressure in both laminar and turbulent flow regimes. At the same time, it increases the friction coefficient in the ML area and reduces the friction coefficient in the HL area and needs higher speed to change from mixed lubrication to hydrodynamic lubrication.

AUTHOR DECLARATIONS

Conflict of Interest

The authors have no conflicts to disclose.

DATA AVAILABILITY

The data that support the findings of this study are available from the corresponding author upon reasonable request.

APPENDIX: DERIVATION OF THE REYNOLDS EQUATION CONSIDERING TURBULENCE AND CAVITATION

Figure 18 shows a schematic diagram of bearing oil film thickness considering the surface roughness of journal and bush. The upper surface velocity is U, and the lower surface velocity is zero.
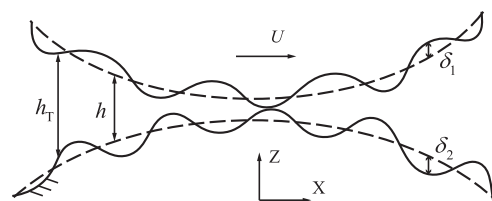

FIG. 18. Oil film thickness of bearing with rough surfaces.

18 September 2023 09:20:15

According to Ref. 9, considering turbulence and the surface roughness of bearing and journal, the average unit volume flow in the x and y directions is

$$\begin{cases} \overline{q}_x = \dfrac{1}{\Delta y} \displaystyle\int_y^{y+\Delta y} \left(-\dfrac{h_T^3}{k_x \eta} \dfrac{\partial \tilde{p}}{\partial x} + \dfrac{U h_T}{2} \right) dy, \\[3mm] \overline{q}_y = \dfrac{1}{\Delta x} \displaystyle\int_x^{x+\Delta x} \left(-\dfrac{h_T^3}{k_y \eta} \dfrac{\partial \tilde{p}}{\partial y} \right) dx, \end{cases} \qquad (A1)$$

where h_T is the local film thickness, $\tilde{p}$ is the hydrodynamic pressure, and δ_1 and δ_2 are the roughness amplitudes.

According to Refs. 7 and 26, Eq. (A1) can be described as

$$\begin{cases} \overline{q}_x = -\phi_x \dfrac{h^3}{k_x \eta} \dfrac{\partial p}{\partial x} + \phi_c \dfrac{Uh}{2} + \phi_s \dfrac{U\sigma}{2}, \\[3mm] \overline{q}_y = -\phi_y \dfrac{h^3}{k_y \eta} \dfrac{\partial p}{\partial y}. \end{cases} \qquad (A2)$$

The flow continuity equation is

$$\frac{\partial(\rho \overline{q}_x)}{\partial x} + \frac{\partial(\rho \overline{q}_y)}{\partial y} = 0, \qquad (A3)$$

where ρ is the density of lubrication oil, which is a constant value.

By substituting Eq. (A2) into Eq. (A3), the average Reynolds equation considering turbulence under the Reynolds condition can be obtained as

$$\frac{\partial}{\partial x}\left(\phi_x \frac{\rho h^3}{k_x \eta} \frac{\partial p}{\partial x} \right) + \frac{\partial}{\partial y}\left(\phi_y \frac{\rho h^3}{k_y \eta} \frac{\partial p}{\partial y} \right) = \phi_c \frac{U}{2}\frac{\partial(\rho h)}{\partial x} + \frac{U\sigma}{2}\frac{\partial(\rho \phi_s)}{\partial x}. \qquad (A4)$$

According to the cavitation algorithm proposed by Payvar and Salant,[21] the expression of Eq. (A4) can be written as

$$\begin{cases} \dfrac{\partial}{\partial x}\left(\phi_x \dfrac{\rho h^3}{k_x \eta} \dfrac{\partial p}{\partial x} \right) + \dfrac{\partial}{\partial y}\left(\phi_y \dfrac{\rho h^3}{k_y \eta} \dfrac{\partial p}{\partial y} \right) = \dfrac{\phi_c U}{2}\dfrac{\partial(\rho h)}{\partial x} + \dfrac{U\sigma}{2}\dfrac{\partial(\rho \phi_s)}{\partial x}, & \text{Liquid film,} \\[3mm] \dfrac{\partial}{\partial x}\left(\dfrac{\rho_v}{\rho} h \right) = 0, & \text{Cavitation zone,} \end{cases} \qquad (A5)$$

where ρ_v is the density of lubrication oil in the cavitation zone, representing the average density of the two-phase flow.

The parameters[21] are defined as follows:

$$\frac{p - p_c}{p_{ref} - p_c} = F\phi, \qquad (A6)$$

$$\frac{\rho_v}{\rho} = 1 + (1 - F)\phi, \qquad (A7)$$

$$F = \begin{cases} 1, & \phi > 0, \\ 0, & \phi < 0. \end{cases} \qquad (A8)$$

By substituting Eqs. (A6)–(A8) into Eq. (A5), the modified average Reynolds equation considering turbulence and cavitation is

$$\frac{\partial}{\partial x}\left(\phi_x \frac{h^3}{k_x} \frac{\partial(F\phi)}{\partial x} \right) + \frac{\partial}{\partial y}\left(\phi_y \frac{h^3}{k_y} \frac{\partial(F\phi)}{\partial y} \right)$$
$$= \frac{\phi_c \eta U}{2(p_{ref} - p_c)} \frac{\partial\{[1 + (1 - F)\phi]h\}}{\partial x} + \frac{\eta U F \sigma}{2(p_{ref} - p_c)} \frac{\partial \phi_s}{\partial x}. \qquad (A9)$$

REFERENCES

[1] J. Sun and C. L. Gui, "Hydrodynamic lubrication analysis of journal bearing considering misalignment caused by shaft deformation," Tribol. Int. **37**(10), 841–848 (2004).

[2] B. Manser, I. Belaidi, A. Hamrani et al., "Performance of hydrodynamic journal bearing under the combined influence of textured surface and journal misalignment: A numerical survey," C. R. Mec. **347**(2), 141–165 (2019).

[3] X. Guo, Y. F. Han, J. X. Wang et al., "A transient hydrodynamic lubrication comparative analysis for misaligned micro-grooved bearing considering axial reciprocating movement of shaft," Tribol. Int. **132**, 11–23 (2019).

[4] J. Ma, C. Fu, H. Zhang et al., "Modelling non-Gaussian surfaces and misalignment for condition monitoring of journal bearings," Measurement **174**, 108983 (2021).

[5] J. Jang and M. Khonsari, "On the characteristics of misaligned journal bearings," Lubricants **3**(1), 27–53 (2015).

[6] A. de Kraker, R. A. J. van Ostayen, and D. J. Rixen, "Calculation of Stribeck curves for (water) lubricated journal bearings," Tribol. Int. **40**(3), 459–469 (2007).

[7] N. Patir and H. S. Cheng, "An average flow model for determining effects of three-dimensional roughness on partial hydrodynamic lubrication," J. Lubr. Technol. **100**(1), 12–17 (1978).

[8] F. Lv, Z. Rao, N. Ta et al., "Mixed-lubrication analysis of thin polymer film overplayed metallic marine stern bearing considering wall slip and journal misalignment," Tribol. Int. **109**, 390–397 (2017).

[9] F. Lv, C. Jiao, N. Ta et al., "Mixed-lubrication analysis of misaligned bearing considering turbulence," Tribol. Int. **119**, 19–26 (2018).

[10] V. N. Constantinescu, "Analysis of bearings operating in turbulent regime," J. Basic Eng. **84**(1), 139–151 (1962).

[11] C.-W. Ng and C. H. T. Pan, "A linearized turbulent lubrication theory," J. Basic Eng. **87**(3), 675–682 (1965).

[12] H. G. Elrod and C. W. Ng, "A theory for turbulent fluid films and its application to bearings," J. Lubr. Technol. **89**(3), 346–362 (1967).

[13] G. G. Hirs, "A bulk-flow theory for turbulence in lubricant films," J. Lubr. Technol. **95**(2), 137–145 (1973).

[14] S. Dousti, P. Allaire, T. Dimond et al., "An extended Reynold equation applicable to high reduced Reynolds number operation of journal bearings," Tribol. Int. **102**, 182–197 (2016).

[15] H. Feng, S. Jiang, and A. Ji, "Investigations of the static and dynamic characteristics of water-lubricated hydrodynamic journal bearing considering turbulent, thermohydrodynamic and misaligned effects," Tribol. Int. **130**, 245–260 (2019).

[16] R. Awasthi and J. S. Maan, "Influence of surface texture on the performance of hydrodynamic journal bearing operating under turbulent regime," Tribol. Online **16**(2), 99–112 (2021).

[17] M. J. Braun and W. M. Hannon, "Cavitation formation and modelling for fluid film bearings: A review," Proc. Inst. Mech. Eng., Part J **224**(9), 839–863 (2010).

[18] B. Jakobsson and L. Floberg, "The finite journal bearing, considering vaporization," Trans. Chalmers Univ. Technol. **190**, 1–116 (1957).

[19] K. O. Olsson, "Cavitation in dynamically loaded bearings," Trans. Chalmers Univ. Technol. **308**, 1–60 (1965).

[20] H. G. Elrod, "A cavitatison algorithm," J. Tribol. **103**(3), 350–354 (1981).

[21] P. Payvar and R. F. Salant, "A computational method for cavitation in a wavy mechanical seal," J. Tribol. **114**(1), 199–204 (1992).

[22] J. Y. Jang and M. M. Khonsari, "On the behavior of misaligned journal bearings based on mass-conservative thermohydrodynamic analysis," J. Tribol. **132**(1), 011702 (2010).

[23] T. He, D. Zou, X. Lu *et al.*, "Mixed-lubrication analysis of marine stern tube bearing considering bending deformation of stern shaft and cavitation," Tribol. Int. **73**, 108–116 (2014).

[24] X. Lin, S. Jiang, C. Zhang *et al.*, "Thermohydrodynamic analysis of high speed water-lubricated spiral groove thrust bearing considering effects of cavitation, inertia and turbulence," Tribol. Int. **119**, 645–658 (2018).

[25] D. Vijayaraghavan and T. G. Keith, "Effect of cavitation on the performance of a grooved misaligned journal bearing," Wear **134**(2), 377–397 (1989).

[26] C. Wu and L. Zheng, "An average Reynolds equation for partial film lubrication with a contact factor," J. Tribol. **111**(1), 188–191 (1989).

[27] J. A. Greenwood and J. H. Tripp, "The contact of two nominally flat rough surfaces," Proc. Inst. Mech. Eng. **185**(1), 625–633 (1970).

[28] D. E. Sander, H. Allmaier, H. H. Priebsch *et al.*, "Edge loading and running-in wear in dynamically loaded journal bearings," Tribol. Int. **92**, 395–403 (2015).

[29] N. Patir and H. S. Cheng, "Application of average flow model to lubrication between rough sliding surfaces," J. Lubr. Technol. **101**(2), 220–229 (1979).

18 September 2023 09:20:15